Hindawi
Mathematical Problems in Engineering
Volume 2019, Article ID 7830489, 11 pages
https://doi.org/10.1155/2019/7830489

Research Article

Uncertainty Estimation of Robot Geometric Parameters and End-Effecter Position Based on New Generation GPS

Xiulan Wen[1], **Shun He**[1], **GuiFang Qiao**[1], **Dongxia Wang**[1], **Aiguo Song**[2], **ChuanShuai Kang**[1] and **Zhongyan Lv**[1]

[1]*Automation Department, Nanjing Institute of Technology, Nanjing 211167, China*
[2]*School of Instrument Science and Engineering, Southeast University, Nanjing 210096, China*

Correspondence should be addressed to Xiulan Wen; zdhxwxl@njit.edu.cn

Received 6 January 2019; Revised 7 April 2019; Accepted 14 April 2019; Published 9 June 2019

Academic Editor: Jixiang Yang

The robot end-effecter positioning accuracy can be improved by the calibration of robot geometric parameters errors. According to the requirements of new generation geometrical product specification (GPS), the calibration uncertainty should be given when the calibration results are given. In this paper, the modified Denavit-Hartenberg method (MDH) of six-joint series robot is established and the joint movement trajectory method is applied to calibrate the robot geometric parameters. The uncertainty contributors significant are analyzed and the calibration uncertainty of robot geometric parameters is estimated based on the guide to the expression of uncertainty in measurement (GUM). In order to overcome the limitations of GUM for highly nonlinear model and reduce computational cost based on Monte Carlo Simulation (MCS) error estimation, an adaptive MCS (AMCS) is proposed to estimate the uncertainty distribution of robot end-effector position. Simulation and practical example are illustrated and the experiments results confirm that not only can the proposed method evaluate the calibration uncertainty of geometric parameters, but also the uncertainty distribution of end-effecter positions in the whole robot workspace can be estimated by AMCS in which the number of MCS trials can be selected adaptively and the quality of the numerical results can be controlled directly. The proposed method not only can evaluate the uncertainty of six-joint series robot geometric parameters and end-effecter position rapidly and accurately, but also can be popularized to the estimation of calibration uncertainty of other kinds of robot geometric parameters.

1. Introduction

The main indexes of industrial robot positioning performance are repetitive positioning accuracy and absolute positioning accuracy [1]. Now most industrial manufacturers adopt the ISO 9283 norm [2], but the only upfront information regarding the positioning performance of an industrial robot continues to be a single measure specified as something like "positioning performance according to ISO 9283," which actually refers to the average unidirectional position repeatability and accuracy at five poses obtained from thirty cycles [3, 4]. If the robot end-effector poses are manually taught, repetitive positioning accuracy is all that matters. The demand for industrial robots with higher absolute positioning accuracy has been growing continuously, especially in the fields of aerospace, medical treatment, and robot-assisted measurement, where positions are defined in a virtual space with respect to an absolute or relative coordinate system. Based on investigation of the error contribution from various sources, the robot geometric errors are responsible for about 90% of the total positioning error [5]. Therefore, many scholars have devoted to the study on geometric parameters calibration to improve absolute positioning accuracy [4–9]. The absolute accuracy of an ABB IRB1600 industrial robot was improved by using a 29-parameter calibration model which takes into account all possible geometry errors. The least squares optimization technique was developed to find the 29 error parameters that best fit the measures acquired with a laser tracker [4]. In order to improve the absolute positioning accuracy of an industrial robot with a parallelogram mechanism, Guo et al. proposed a multilevel calibration technique [6]. Joubair and Bonev developed a geometric calibration method based on sphere and distance constraints to improve the accuracy of a

six-axis serial industrial robot in a specific target workspace [7]. Möller et al. presented an approach for increasing the absolute positioning accuracy of an industrial milling robot with help of a stereo camera system [8]. Nubiola presented the successful use of this measurement system for absolute robot calibration and the mean absolute positioning error was improved from 0.873 mm to 0.479 mm [9]. Wu et al. dealt with geometric calibration of industrial robots and focused on the reduction of the measurement noise impact by means of proper selection of the manipulator configurations in calibration experiments. The geometric calibration results for a KUKAKR-270 industrial robot showed that manipulator positioning accuracy was 5.5 times better compared to the noncalibrated robot [10].

In terms of metrology based on new generation GPS, the measurement results must be given with a quantitative evaluation of their accuracy with measurement uncertainty [11]. Different approaches [12–17] have been proposed to quantify the uncertainty caused by measurement, modeling of complex physical systems or fuzzy systems. Among them, GUM [18, 19] is a highly practical and easily implement approach for cases where the measurement model is linear and the probability distribution of the output is normal distribution. It provides an analytical methodology for assessing and reporting the measurement uncertainty and can be applied to most fields of physical measurements. However, when the physical model is complex or the probability distribution of the output is significantly asymmetric, the GUM method to evaluate the measurement uncertainty will result in the inaccurate results. Supplement 1 to the GUM (GUM S1) is recommended by the Joint Committee for Guides in Metrology (JCGM) [20] which is implemented by Monte Carlo Simulation. ISO/TS15530 states that the most effective method for estimating uncertainty is computer simulation, and more specifically, a Monte Carlo simulation [21].

Calibrations are measurements which determine quantity values. Because calibration devices, calibration standards, reagents, and tools are not perfect, environmental conditions, processes, procedures, and people are also imperfect and variable, each calibration has uncertainty associated with it [19]. According to new generation GPS, the calibration results must be given with a quantitative evaluation of their accuracy. Therefore, the study on the evaluation of calibration uncertainty of robot geometric parameters has drawn the attention of scholars and several researches have been reported [22–24]. Santolaria and Ginés presented Monte Carlo method to evaluate the uncertainty for a robot arm calibrated [22]. Li and Qu used GUM to evaluate the calibration uncertainty of geometric parameters [23]. Olarra and Axinte proposed a calibration method which enabled completely automatic identification of the kinematics of a walking hexapod robotic machine tool and proposed an analytical methodology to estimate the uncertainty of the identified geometric parameters [24].

To estimate the calibration uncertainty of robot geometric parameters and end-effector position, the remainder of this paper is organized as follows. In Section 2, the model of robot geometric parameters is established. The calibration procedure of geometric parameters and the calculation method of the end-effector position are given. In Section 3, The GUM method is used to calculate the calibration uncertainty of robot geometric parameters. AMCS for the uncertainty estimation of robot end-effector position is developed and the flowchart of AMCS is given. In Section 4, simulation and practical example are given. The uncertainty contributors significant are analyzed. And the calibration uncertainties of geometric parameters and end-effector position are estimated. Finally, conclusions are reached in Section 5.

2. Geometric Parameters Calibration and End-Effector Position Calculation

2.1. Geometric Parameters Calibration

2.1.1. Robot Geometric Model. A number of different approaches including Denavit-Hartenberg (DH) method, S model method, Complete and Parametrically Continuous (CPC) model method, zero reference model method, and Product of Exponentials (POE) formula method exist for developing the geometric model of a robot manipulator [25]. The most popular model has been the DH model which is based on homogeneous transformation matrices [3]. This procedure consists of establishing coordinate systems on each joint axis. Each coordinate system is then related to the next through a specific set of coefficients in the homogeneous transformation matrices. To be suitable for robot calibration, the robot geometric model must satisfy three basic requirements: model completeness, parameter minimality, and model continuity. The conventional DH is not enough to achieve a complete model for geometric parameters calibration. In addition, when the adjacent joint axes are parallel, little changes at this state may cause dramatic changes at the common perpendicular between the two axes. The changes may result in robot singularity, which lead to discontinuity of the geometric model. Therefore, a modified DH (MDH) method was proposed, the core of which was to add an angle parameter to the DH model to describe the position relationship between adjacent parallel axes, to cancel the incompleteness problem [25–27]. In this paper, MDH model is adopted to establish the geometric parameters model of six-joint series robot for avoiding the singularity of conventional DH model.

2.1.2. Acquisition of Joint Axis Space Position. For obtaining the spatial position of the robot joint axis, each axis is controlled to move separately and the target ball position is measured by the laser tracker. The spatial plane in which the trajectory is located is fitted.

Supposing that the coordinates of measured points are $P_j(x_j, y_j, z_j)$, $j = 1, 2, \cdots n$, n is the number of measured points. The space plane equation is expressed as

$$Ax + By + Cz + 1 = 0 \tag{1}$$

$\boldsymbol{X} = [A\ B\ C]^{\mathrm{T}}$ is the normal vector of the plane, which is also the direction vector $\boldsymbol{n}$ of the robot joint axis.

Equation (1) can be rewritten as a matrix form:

$$\boldsymbol{SX} = \boldsymbol{L} \tag{2}$$

where $\boldsymbol{S} = \begin{bmatrix} x_1 & y_1 & z_1 \\ \vdots & \vdots & \vdots \\ x_n & y_n & z_n \end{bmatrix}$, $\boldsymbol{L} = \begin{bmatrix} -1 \\ \vdots \\ -1 \end{bmatrix}$,

To solve (2) by using the least square method, we have

$$\boldsymbol{X} = \left(\boldsymbol{S}^T\boldsymbol{S}\right)^{-1}\boldsymbol{S}^T\boldsymbol{L} \tag{3}$$

The trajectory of axis is a space circle whose center and radius are solved by using the space projection method [28] and its objective function is expressed as

$$\begin{aligned} &F\left(x_0, y_0, z_0, R, \lambda\right) \\ &= \sum_{j=1}^{n}\left[\left(x_j' - x_0\right)^2 + \left(y_j' - y_0\right)^2 + \left(z_j' - z_0\right)^2 - R^2\right] \\ &\quad + \lambda\left(Ax_0 + By_0 + Cz_0 + 1\right) \end{aligned} \tag{4}$$

where $P_j'(x_j', y_j', z_j')$ is the projection point of $P_j(x_j, y_j, z_j)$ on the fitting plane, (x_0, y_0, z_0) and R are the coordinates of sphere center and sphere radius, respectively. λ is a spatial constraint coefficient. (x_0, y_0, z_0) and R can be obtained by using the extremum method. Therefore, the spatial position of joint axis can be determined by the plane normal vector $\boldsymbol{X}$ and sphere center coordinates (x_0, y_0, z_0).

2.1.3. Establishment of Coordinate System. The coordinate system $\{T_i\}$ (i = 1, 2, ..., H, H is the number of joints) of nonparallel joints is established based on the axis equations of joint i (J_i) and joint i+1 (J_{i+1}) and shown in Figure 1. The axis direction vector $\boldsymbol{n}_{i+1}$ of J_{i+1} is set to the axis z_i. The common perpendicular of the axes of J_i and J_{i+1} is set to the axis x_i. The intersection of the axes x_i and z_i is the origin O_i. The axis y_i is obtained by the right hand rule: $y_i = z_i \times x_i$. C_i is the center of axis trajectory when J_i rotates separately.

For parallel joints the joint coordinate system $\{T_{i-1}\}$ and the axis direction vector $\boldsymbol{n}_{i+1}$ of J_{i+1} are shown in Figure 2. The intersection of the auxiliary plane $Ax + By + Cz + 1 = 0$ and the axis of J_{i+1} is the origin O_i of the coordinate system $\{T_i\}$. The auxiliary vector $\boldsymbol{h}$ is the unit one from O_{i-1} to O_i. The vector $\boldsymbol{n}_{i+1}$ is set to the axis z_i. The common perpendicular of vector $\boldsymbol{h}$ and the axis z_i is set to y_i. The axis x_i is obtained by the right-hand rule: $x_i = z_i \times y_i$.

2.1.4. Calibration Procedure. The MDH method is used to establish the geometric model of six-joint series robot, in which the parameters are link length a_i, offset distance d_i, joint angle θ_i, and joint torsion angle α_i and β_i. α_i expresses the rotation angle from the axis $\boldsymbol{z}_i$ to $\boldsymbol{z}_{i+1}$ around the axis $\boldsymbol{x}_i$ and β_i is the rotation angle from the axis $\boldsymbol{z}_i$ to $\boldsymbol{z}_{i+1}$ around the axis $\boldsymbol{y}_i$. The actual values of geometric parameters $a_i, d_i, \theta_i, \alpha_i$, and β_i can be calibrated according to the conversion relation between the coordinate systems of robot adjacent joints and their geometry definition. The calibration flow is as follows.

Step 1. Install the target ball of laser tracker at the robot end-effector and set the robot at the initial zero position.

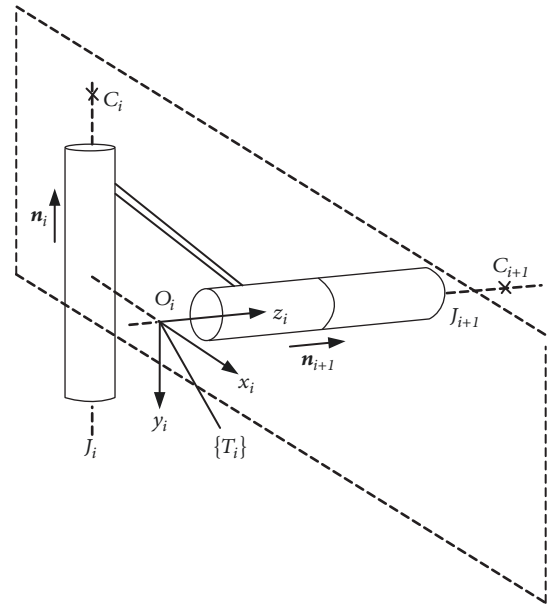

Figure 1: Coordinate system establishment for nonparallel joints.

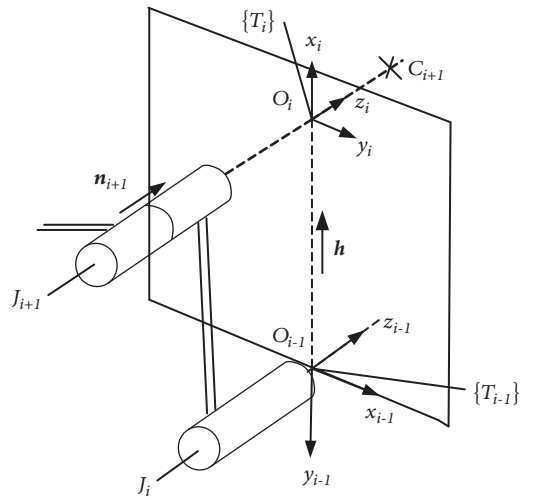

Figure 2: Coordinate system establishment for parallel joints.

Step 2. Control the first joint to rotate in a measurable range and measure the target ball position by using laser tracker. Control this joint to return to the initial zero position after the motion of axis ends. Then, control the next joint to rotate separately until the last one. The target ball position of each joint is measured and the data are recorded.

Step 3. Fit the trajectory circle C_i of each joint i by Spatial Analyzer (SA) software provided by Leica laser tracker and calculate the normal vector $\boldsymbol{X_i}$ of the plane in which the space circle lies.

Step 4. Establish the coordinate system of each joint according to Section 2.1.3. Calculate and obtain the calibrated

geometric parameters of each joint according to the geometry definition.

2.2. Calculation of Robot End-Effector Position. Based on the MDH method, the translation matrix ${}^{i-1}_{i}T$ from the $i-1$ coordinate to i coordinate can be calculated as [26]

$$\begin{aligned}
&{}^{i-1}_{i}\boldsymbol{T} \\
&= Rot(z,\theta_i) * Trans(z,d_i) * Trans(x,a_i) * Rot(x,\alpha_i) \\
&\quad * Rot(y,\beta_i) \\
&= \begin{bmatrix} c\theta_i c\beta_i - s\theta_i s\alpha_i s\beta_i & -s\theta_i c\alpha_i & c\theta_i s\beta_i + s\theta_i s\alpha_i c\beta_i & a_i c\theta_i \\ s\theta_i c\beta_i + c\theta_i s\alpha_i s\beta_i & c\theta_i c\alpha_i & s\theta_i s\beta_i - c\theta_i s\alpha_i c\beta_i & a_i s\theta_i \\ -c\alpha_i s\beta_i & s\alpha_i & c\alpha_i c\beta_i & d_i \\ 0 & 0 & 0 & 1 \end{bmatrix}
\end{aligned} \tag{5}$$

where c and s stand for cos and sin, respectively. When the adjacent joints are parallel or near parallel, $d_i = 0$, or else $\beta_i = 0$.

The transformation matrix from the base coordinate to the end effector can be expressed as

$${}^{0}_{N}T = \prod_{i=1}^{H} {}^{i-1}_{i}T = \begin{bmatrix} n_x & o_x & a_x & P_x \\ n_y & o_x & a_x & P_y \\ n_z & o_z & a_z & P_z \\ 0 & 0 & 0 & 1 \end{bmatrix} \tag{6}$$

From (5) and (6) it is shown that the end-effector position $P = [P_x \ P_y \ P_z]^{\mathrm{T}}$ can be calculated by the geometric parameters a_i, d_i, θ_i, α_i, and β_i $(i = 1, 2, \ldots, H)$ and be expressed as

$$P = f(a_i, \alpha_i, d_i, \beta_i, \theta_i) \tag{7}$$

It can be seen that the functional relationship between the robot geometric parameters and its end-effector position is highly nonlinear.

3. Uncertainty Estimation

Measurement uncertainty is a nonnegative parameter characterizing the dispersion of the quantity values being attributed to a measurand based on the information used. GUM is the internationally accepted master document for evaluating uncertainty and it requires the use of a first-order Taylor series expansion for propagating uncertainties. When the mathematical model of measurand is highly nonlinear the use of this linear approximation may be inadequate, MCS is recommended. Furthermore, in order to ensure the stability of required results, the adaptive MCS allows adjusting the number of MCS trials [20].

3.1. Uncertainty Estimation of Geometric Parameters. According to the GUM method, the uncertainty of the measurement results generally includes several components, which can be classified into Type-A and Type-B uncertainties based on the numerical evaluation methods. Type-A uncertainty is evaluated by statistical approach and characterized by the experimental standard deviation. Type-B uncertainty is obtained by nonstatistical approach and characterized by empirical or standard deviation estimated from the assumed probability distribution. For the situation with sufficient and independent test data, Type-A uncertainty is more objective than other techniques for uncertainty quantification [19]. A series of measurements are conducted and the standard deviation of tests is obtained; then Type-A uncertainty can be represented as

$$u_A = u(\bar{b}) = \sqrt{\frac{\sum_{i=1}^{N} (b_i - \bar{b})^2}{N(N-1)}} \tag{8}$$

where N is the test times, b_i represents the result of the ith test, and $\bar{b}$ represents the mean-value of b_i $(i = 1, 2, \ldots, N)$. In our experiments, Type-A uncertainty is used to calculate the calibration uncertainty of robot geometric parameters [23].

3.2. Uncertainty Estimation of Robot End-Effector Position

3.2.1. MCS. Typically, a measurand Y is not measured directly and it is determined by m other quantities $X_1, X_2, \ldots, X_m$ through a functional relationship f:

$$Y = f(X_1, X_2, \ldots, X_m) \tag{9}$$

If the functional relationship between Y and its input quantities X_i $(i = 1, \ldots, m)$ is highly nonlinear and a first-order Taylor expansion of the relationship is not an acceptable approximation, in such cases, MCS is required to evaluate the uncertainty [20]. The heart of MCS is repeatedly sampling from probability density function (PDF) for X_i $(i = 1, \ldots, m)$ and evaluating model (9) in each case.

MCS can be summarized as follows.

(1) Set the number M of MCS to be conducted.

(2) Generate M vectors by sampling from the assigned PDFs, as realizations of the set of m input quantities X_i.

(3) Form the corresponding model value of Y and yield M model values for each such vector.

(4) Sort these M model values into strictly increasing order and use the sorted model values to provide the distribution function G.

(5) Use G to form an estimate y of Y and the standard uncertainty $u(y)$ associated with y.

(6) Use G to form an appropriate coverage interval for Y for a stipulated coverage probability p.

3.2.2. Uncertainty Estimation of End-Effector Position Based on AMCS. It can be seen that the number M of MCS needs to be selected in advance and there is no direct control over the quality of the numerical results provided by MCS. It cannot guarantee that any specific preassigned number M will suffice. As the Monte Carlo trials increases, the average quality of the system is improved by decreasing the statistical uncertainty of the quantities of interest. The statistical reliability of the measurement uncertainty evaluated by MCS is

of utmost importance and AMCS is an effective method to ensure the calculation reliability.

From (5), (6), and (7) we can see that the relationship of the end-effector position $P(P_x, P_y, P_z)$ and the geometric parameters $a_i, d_i, \theta_i, \alpha_i$, and β_i $(i = 1, 2, \ldots, H)$ is highly nonlinear. Considering that a fixed number M cannot guarantee the reliability of the calibration uncertainty for robot end-effector position, AMCS is proposed to estimate the uncertainty of robot end-effector position. A basic implementation of AMCS involves carrying out an increasing number of MCS trials until the important results such as expected value P, standard uncertainty $u(P)$, and lower and higher coverage interval endpoints P_{low} and P_{high} have stabilized if twice their standard deviations are equal or smaller than the associated numerical tolerance δ, which relies on the number n_{dig} of significant digits of the results [17, 20]. The AMCS flowchart for uncertainty estimation of robot end-effector position is shown in Figure 3.

4. Results and Discussion

4.1. Simulation. In order to analyze the effect of robot geometric parameters errors on the uncertainty distributions of end-effector position, the geometric parameters nominal values of AIFUTE ER10L-C10 industrial robot are shown in Table 1. When six-joint angles are 0°, -90°, 0°, 0°, 0°, 0°, respectively, the robot is at the initial zero position. 1000 random errors obeying the Gaussian distribution with mean 0 and standard deviation 0.1mm are generated and added to the nominal values d_i and a_i, respectively. 1000 random errors obeying Gaussian distribution with mean 0 and standard deviation 0.01rad and 0.001rad are generated and added to the nominal values θ_i, α_i, and β_i, respectively. End-effector positions are calculated according to (5) and (6). And the uncertainty distributions of three-dimensional space of robot end-effector are shown in Figures 4(a) and 4(b), respectively. Comparing Figures 4(a) and 4(b), it can be seen that geometric parameters errors directly influence the absolute positioning accuracy of robot end-effector. The smaller angle parameters errors result in larger uncertainty distribution of robot end-effector position.

For further analyzing the effect of each parameter on the end-effector position, 1000 random errors obeying above Gaussian distribution are added to each nominal geometric parameter separately and the end-effector positions are calculated. We find that the angle parameters have much more effect on the uncertainty distribution of end-effector positions than the length parameters. Moreover, the joint angle θ_i has much more effect on end-effector positions than joint torsion angle α_i. The separate effects of joint angle θ_i and torsion angle α_i on the uncertainty distribution of the end-effector position are shown in Figures 4(c) and 4(d), respectively.

4.2. Experimental Setup. As case study, AIFUTE ER10L-C10 robot was used for calibration experiments. The experimental setup was shown in Figure 5, where Leica 930 laser tracker was used and the target ball was installed at the robot end-effector. Assume that the method was able to locate at the exact position of the robot end-effector in the base frame coordinates. Therefore, the orientation of robot end-effector was not considered [22].

Point-by-point sampling was adopted and the stable point measurement mode was set in order to reduce the effect of motor vibration. During the process of the robot calibration, the experiments environment such as temperature, humid, vibration, and dust was well controlled [2]. Control each joint to rotate in the same environmental conditions. The target ball positions corresponding to calibrated points were measured by Leica 930 laser tracker.

4.3. The Calibration of Robot Geometric Parameters. Based on the spatial projection method the center and plane normal vector of the space circle are computed and the joint coordinate systems are established. The MDH model is established and the actual parameters are calibrated according to Section 2.1. For comparison the calibrated geometric parameters are also listed in Table 1.

4.4. The Calibration Uncertainty of Geometric Parameters. When laser tracker is used to measure and calibrate the robot geometric parameters, the calibration uncertainty mainly results from measurement equipment (Leica AT930), sampling strategy, joint movement range, and measurement environment.

The standard uncertainties of calibrated geometric parameters are expressed as $u_{ai}, u_{di}, u_{\alpha i}, u_{\theta i}, u_{\beta i}$ $(i = 1, 2, \ldots, 6)$ and their uncertainty contributors significant include the following [29–31].

(1) Repeatability. 30 times repeated measurements are recommended [19] and have been conducted. Type-A uncertainty based upon repeated measurements from a controlled process is used to estimate the standard uncertainties $ur_{\theta i}, ur_{di}, ur_{ai}, ur_{\alpha i}, ur_{\beta i}$ $(i = 1, 2, \ldots, 6)$ from repeatability for the set and their values are shown in Table 2.

(2) Sampling Strategy. Point-by-point sampling strategy is adopted. The robot geometric parameters can be calibrated with a theoretically necessary minimum number of measured points. But how many measured points are needed reliably to calibrate the geometric parameters is an unsolved problem. In our experiments, the number of measured points is set to 100, 80, 60, 50, 40, 25, 20, and 10, respectively. The standard uncertainties $us_{\theta i}, us_{di}, us_{ai}, us_{\alpha i}, us_{\beta i}$ $(i = 1, 2, \ldots, 6)$ resulting from sampling strategy are estimated and their values are shown in Table 3.

(3) Joint Movement Range. Considering the limitations of the robot space motion range and the laser tracker measurable range, six joints are controlled to rotate in the range of ±10°, ±20°, ±30°, ±40°, ±50°, ±60°, respectively. The standard uncertainties $um_{ai}, um_{di}, um_{\alpha i}, um_{\theta i}, um_{\beta i}$ $(i = 1, 2, \ldots, 6)$ resulting from joint movement range are estimated and their values are shown in Table 4.

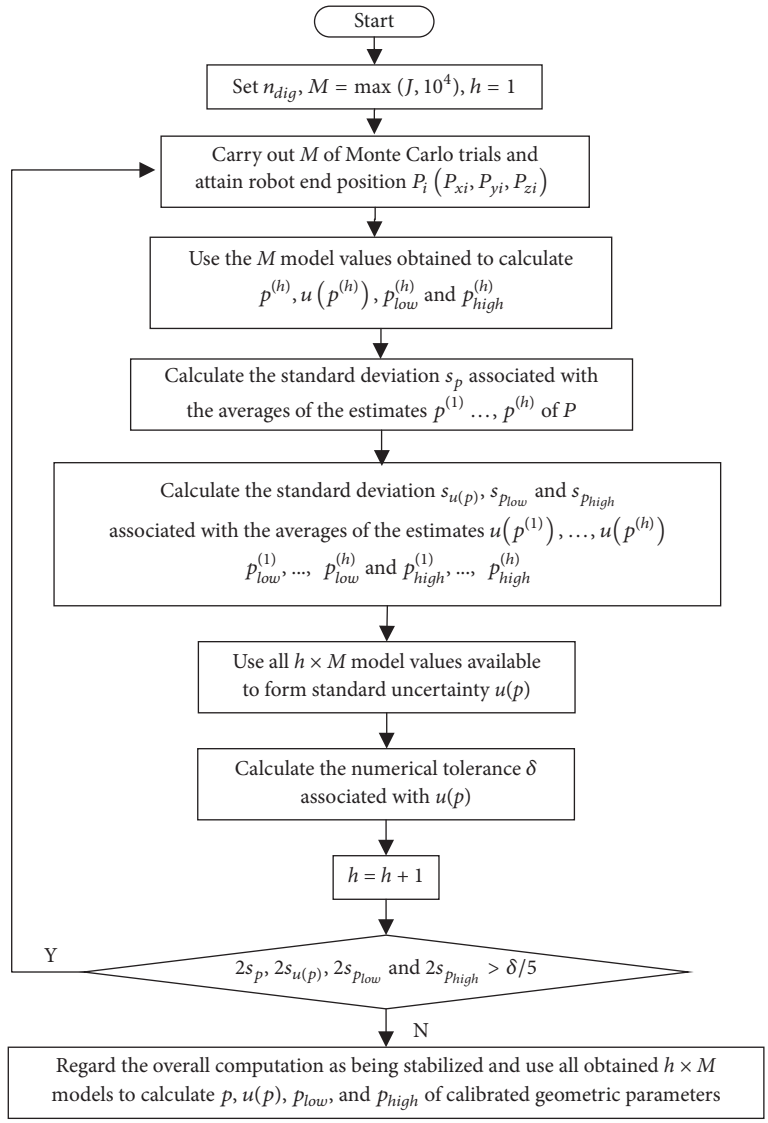

Figure 3: AMCS for uncertainty estimation of end-effector positions.

(4) Measurement Environment. During the robot calibration experiments, the environment such as temperature, humid, and dust was well controlled. In addition, Leica AT930 is equipped with temperature, humidity, and pressure sensors and small changes of temperature, humid, and dust can be compensated in real time. Therefore, the uncertainty from environment is neglected.

Above contributors are considered as uncorrelated; the standard uncertainties $u_{ai}, u_{di}, u_{\alpha i}, u_{\theta i}, u_{\beta i}$ of calibrated geometric parameters can be estimated and shown in Table 1. For example, the uncertainty u_{ai} of link length a_i can be calculated by

$$u_{ai} = \sqrt{ur_{ai}^2 + us_{ai}^2 + um_{ai}^2} \tag{10}$$

The expanded uncertainty U can be obtained by multiplying the standard uncertainty u by coverage factor k:

$$U = ku \tag{11}$$

For calibration and test reports $k = 2$ is commonly used and it provides 95% confidence. When Type-A components have been calculated with 30 repeated measurements or more this value is appropriate [19]. For comparison, the upper endpoint (U-endpoint) and lower endpoint (L-endpoint) of 95% coverage intervals for calibrated geometric parameters are also listed in Table 1.

4.5. The Uncertainty of the Robot End-Effector Position. In order to investigate the calibration uncertainty of geometric parameters effect on the end-effector position, AMCS is carried out to estimate the uncertainty of the robot end-effector position. Geometric parameter errors obeying the Gaussian distribution in which the mean is the calibrated value of each geometric parameter and standard deviation is its uncertainty are generated. The robot end-effector positions can be calculated by(6). In the application of AMCS, the confidence probability p and numerical tolerance δ are set to

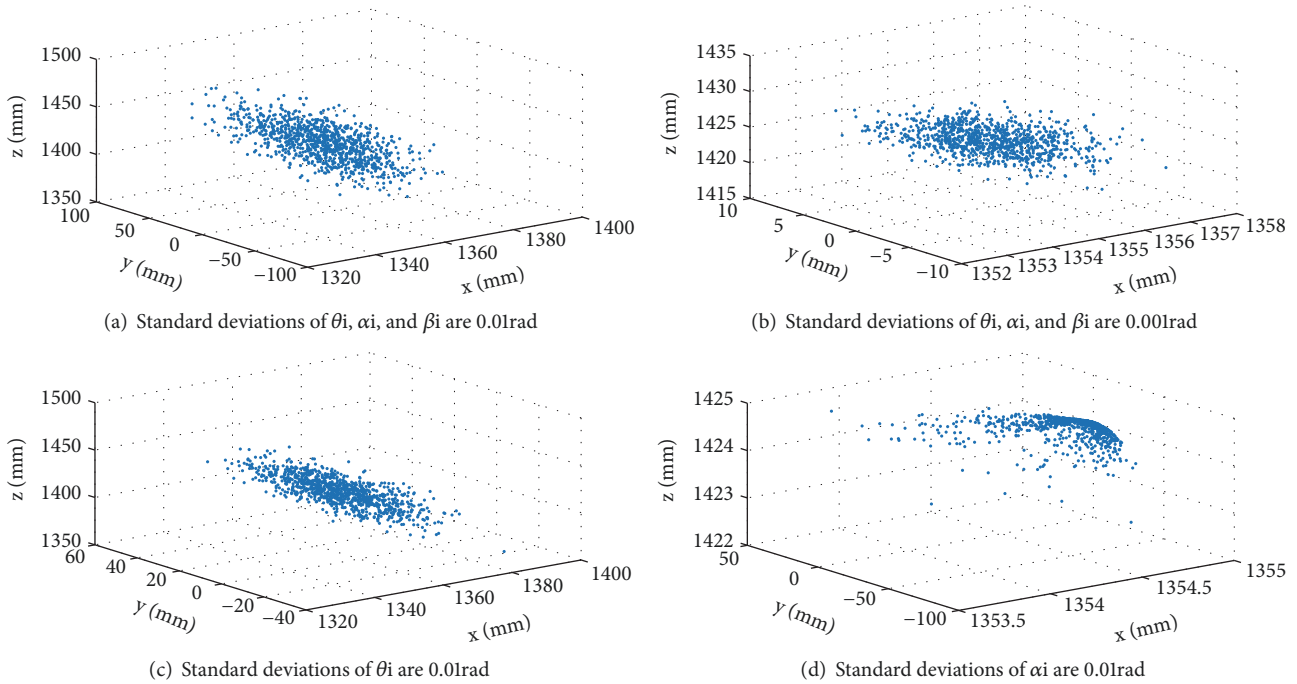

Figure 4: The uncertainty distributions of robot end-effector by simulation.

Table 1: The calibrated values, uncertainty, and the endpoints of 95% coverage intervals of geometric parameters.

Parameters	Nominal values	Calibrated values	Uncertainty	Expanded uncertainty	U-endpoint	L-endpoint
$\theta_1(^\circ)$	0.00	0.0000	0.0000	0.0000	0.0000	0.0000
$\theta_2(^\circ)$	-90.00	-90.0620	0.0112	0.0224	-90.0396	-90.0844
$\theta_3(^\circ)$	0.00	-0.1825	0.0188	0.0376	-0.1449	-0.2201
$\theta_4(^\circ)$	0.00	-0.3125	0.0935	0.1870	-0.1255	-0.4995
$\theta_5(^\circ)$	0.00	-0.5217	0.0146	0.0292	-0.4925	-0.5509
$\theta_6(^\circ)$	0.00	0.0000	0.0000	0.0000	0.0000	0.0000
d_1(mm)	504.00	504.0000	0.0000	0.0000	504.0000	504.0000
d_2(mm)	0.00	0.0000	0.0000	0.0000	0.0000	0.0000
d_3(mm)	0.00	0.7937	0.7233	1.4466	2.2403	-0.6529
d_4(mm)	1060.00	1059.7833	0.4637	0.9274	1060.7107	1058.8559
d_5(mm)	0.00	0.7176	0.0580	0.1160	0.8336	0.6016
d_6(mm)	125.00	125.0000	0.0000	0.0000	125.0000	125.0000
a_1(mm)	170.00	166.5975	0.1664	0.3328	166.9303	166.2647
a_2(mm)	780.00	780.2600	0.0637	0.1274	780.3874	780.1326
a_3(mm)	140.00	140.3917	0.2980	0.5960	140.9877	139.7957
a_4(mm)	0.00	0.1621	0.1490	0.2980	0.4601	-0.1359
a_5(mm)	0.00	0.1015	0.1778	0.3556	0.4571	-0.2541
a_6(mm)	0.00	0.0000	0.0000	0.0000	0.0000	0.0000
$\alpha_1(^\circ)$	-90.00	-90.0003	0.0108	0.0216	-89.9787	-90.0219
$\alpha_2(^\circ)$	0.00	-0.0261	0.0081	0.0162	-0.0099	-0.0423
$\alpha_3(^\circ)$	-90.00	-89.9810	0.0187	0.0374	-89.9436	-90.0184
$\alpha_4(^\circ)$	90.00	90.0605	0.3552	0.7104	90.7709	89.3501
$\alpha_5(^\circ)$	-90.00	-90.0150	0.3361	0.6722	-89.3428	-90.6872
$\alpha_6(^\circ)$	0.00	0.0000	0.0000	0.0000	0.0000	0.0000
$\beta_2(^\circ)$	0.00	0.0234	0.0099	0.0198	0.0432	0.0036

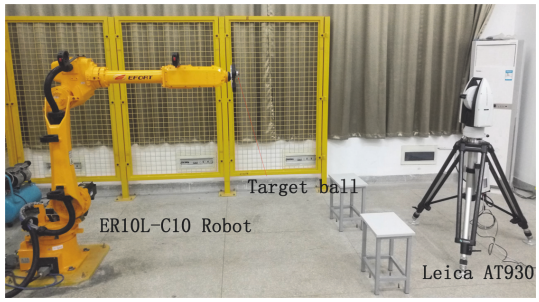

Figure 5: Experimental setup.

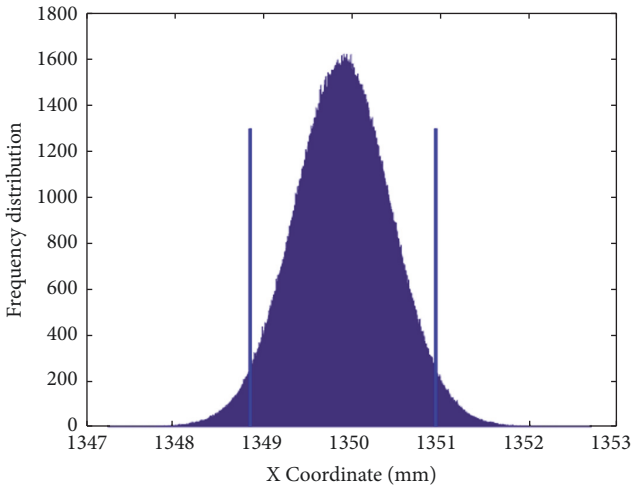

Figure 6: Frequency distributions of X coordinates of the end-effector position.

Table 2: The standard uncertainties from repeatability.

joints	$ur_{\theta i}$ (°)	ur_{di} (mm)	ur_{ai} (mm)	$ur_{\alpha i}$ (°)	$ur_{\beta i}$ (°)
1	0.0000	0.0000	0.0301	0.0007	-
2	0.0043	0.0000	0.0066	0.0014	0.0007
3	0.0019	0.0115	0.0145	0.0010	-
4	0.0032	0.0174	0.0218	0.0060	-
5	0.0060	0.0054	0.0423	0.0059	-
6	0.0000	0.0000	0.0000	0.0000	-

Table 3: The standard uncertainties from sampling strategy.

joints	$us_{\theta i}$ (°)	us_{di} (mm)	us_{ai} (mm)	$us_{\alpha i}$ (°)	$us_{\beta i}$ (°)
1	0.0000	0.0000	0.0218	0.0004	-
2	0.0014	0.0000	0.0128	0.0005	0.0004
3	0.0012	0.0136	0.0053	0.0005	-
4	0.0004	0.0049	0.0016	0.0012	-
5	0.0050	0.0062	0.0012	0.0015	-
6	0.0000	0.0000	0.0000	0.0000	-

0.95 and 0.0001, respectively. The number $M = \max(100/(1 - p), 10^4) = 10^4$. AMCS procedure is run. The frequency distributions of X, Y, and Z coordinates of the robot end-effector are illustrated in Figures 6, 7, and 8, respectively,

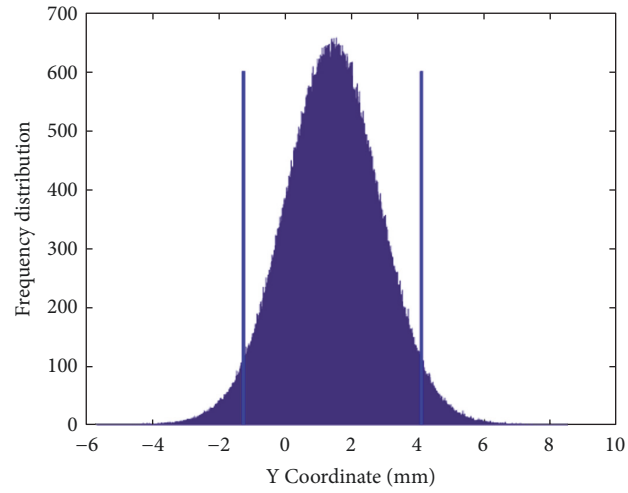

Figure 7: Frequency distributions of Y coordinates of the end-effector position.

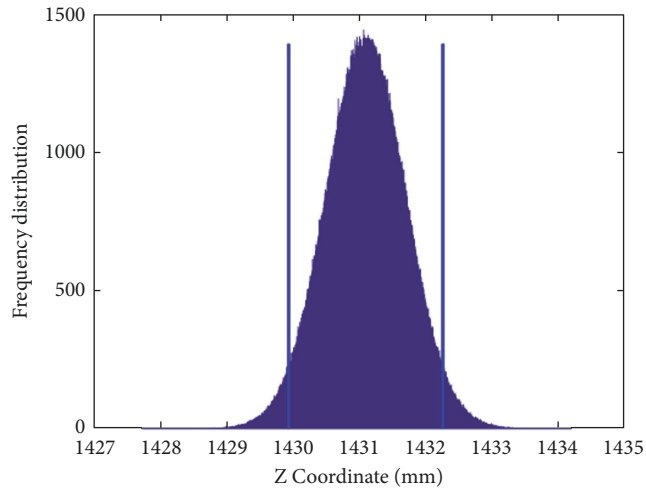

Figure 8: Frequency distributions of Z coordinates of the end-effector position.

Table 4: The standard uncertainties from joint movement range.

joints	$um_{\theta i}$ (°)	um_{di} (mm)	um_{ai} (mm)	$um_{\alpha i}$ (°)	$um_{\beta i}$ (°)
1	0.0000	0.0000	0.1622	0.0108	-
2	0.0103	0.0000	0.0621	0.0080	0.0099
3	0.0187	0.7231	0.2976	0.0187	-
4	0.0934	0.4633	0.1474	0.3551	-
5	0.0123	0.0574	0.1727	0.3360	-
6	0.0000	0.0000	0.0000	0.0000	-

where X_i, Y_i, and Z_i $(i = 1, 2, \ldots, M)$ are assembled into a histogram and it provides an approximation to the PDF of X, Y, and Z. Left and right vertical solid lines express the 95% confidence intervals. From Figures 6, 7, and 8 it can be seen that AMCS involves carrying out an increasing number of MCS trials until the calculation results have stabilized and the frequency distributions of X, Y, and Z coordinates are

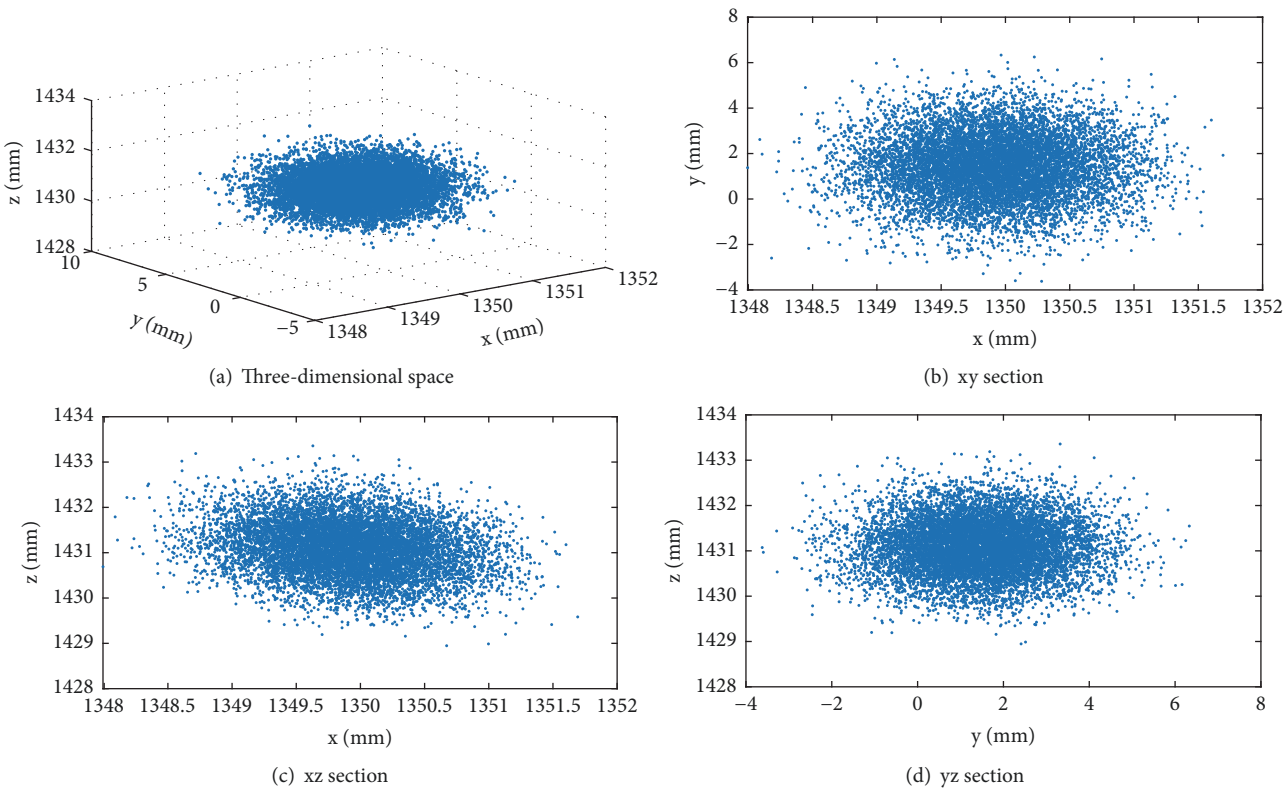

Figure 9: The uncertainty distributions of robot end-effector by experiments.

different. The uncertainty distributions of three-dimensional space, *xy*, *xz*, and *yz* section errors of robot end-effector are shown in Figures 9(a), 9(b), 9(c), and 9(d), respectively.

Comparing Figures 4 and 9, it can be seen that the uncertainty distributions of end-effector position are different due to different geometric parameter errors. And the robot absolute positioning accuracy can be improved by geometric parameters calibration.

5. Conclusions

The MDH method is developed to establish the model of six-joint series robot and the joint movement trajectory method is applied to calibrate the robot geometric parameters. It not only can solve the singularity problem for adjacent joints, but also uses the minimum number of parameters to describe the robot completely. The robot positioning accuracy can be improved by geometric parameters calibration. A series of measurements are conducted and the standard deviation of tests is obtained. The uncertainty components significant for robot geometric parameters calibration by Leica 930 laser tracker are analyzed and the uncertainties are calculated based on GUM. Considering that the functional relationship of the robot end-effector position and geometric parameters is highly nonlinear and the computation time and stability are determined by the number M of MCS trials, AMCS is developed to estimate the uncertainty distribution of end-effector position. It not only can make up for the limitations of GUM for highly nonlinear model, but also has the features that the number of MCS trials can be selected adaptively and the quality of the numerical results can be controlled directly. Simulation and practical example are illustrated and the experiments results verify the proposed method not only can evaluate the uncertainty of geometric parameters, but also estimate the uncertainty distribution of end-effector position in the whole robot workspace. And the uncertainty distribution of end-effector position is greatly affected by geometric parameter errors. It is an effective method to improve the robot absolute positioning accuracy by geometric parameters calibration, especially to reduce angle parameters errors. The proposed method conforms to new generation GPS requirements in which the calibration uncertainty characterizing the reliability of the results is given together when the calibration result is given. It can be popularized to the uncertainty estimation of other kinds of robots' geometric parameters calibration.

Data Availability

The data used to support the findings of this study are available from the corresponding author upon request.

Conflicts of Interest

The authors declare that there is no conflict of interests regarding the publication of this paper.

Acknowledgments

This work was supported by the National Natural Science Foundation of China under Grant No. 51675259, Jiangsu Provincial Natural Science Foundation of China under Grant Nos. BK20170763 and 16KJB460013, Research Innovation Program for College Graduates of Jiangsu Province under Grant No. SJCX18_0581, and Innovation Research of Nanjing Institute of Technology under Grant No. ZKJ201609.

References

[1] B. Greenway, "Robot accuracy," *Industrial Robot: An International Journal*, vol. 27, no. 4, pp. 257–265, 2000.

[2] International Standard Organization, *ISO 9283, Manipulating Industrial Robots - Performance Criteria and Related Test Methods*, ISO Copyright Office, Switzerland, 1998.

[3] S. K. Schröer, *Handbook of Industrial Robotics*, 1999.

[4] A. Nubiola and I. A. Bonev, "Absolute calibration of an ABB IRB 1600 robot using a laser tracker," *Robotics and Computer-Integrated Manufacturing*, vol. 29, no. 1, pp. 236–245, 2013.

[5] A. Elatta, L. Gen, F. Zhi et al., "An overview of robot calibration," *Information Technology Journal*, vol. 3, no. 1, pp. 74–78, 2004.

[6] Y. Guo, S. Yin, Y. Ren, J. Zhu, S. Yang, and S. Ye, "A multilevel calibration technique for an industrial robot with parallelogram mechanism," *Precision Engineering*, vol. 40, pp. 261–272, 2015.

[7] A. Joubair and I. A. Bonev, "Kinematic calibration of a six-axis serial robot using distance and sphere constraints," *The International Journal of Advanced Manufacturing Technology*, vol. 77, no. 1-4, pp. 515–523, 2015.

[8] C. Möller, H. C. Schmidt, N. H. Shah, and J. Wollnack, "Enhanced absolute accuracy of an industrial milling robot using stereo camera system," *Procedia Technology*, vol. 26, pp. 389–398, 2016.

[9] A. Nubiola and I. A. Bonev, "Absolute robot calibration with a single telescoping ballbar," *Precision Engineering*, vol. 38, no. 3, pp. 472–480, 2014.

[10] Y. Wu, A. Klimchik, S. Caro, B. Furet, and A. Pashkevich, "Geometric calibration of industrial robots using enhanced partial pose measurements and design of experiments," *Robotics and Computer-Integrated Manufacturing*, vol. 35, pp. 151–168, 2015.

[11] *Joint Committee for Guides in Metrology. JCGM 100-2008 Evaluation of Measurement Data —Guide to the Expression of Uncertainty in Measurement, GUM 1995 with Minor Corrections*, JCGM Member Organizations (BIPM, IEC, IFCC, ILAC, ISO, IUPAC, IUPAP and OIML), 1st edition, 2008.

[12] D. Xiu and G. E. Karniadakis, "Modeling uncertainty in steady state diffusion problems via generalized polynomial chaos," *Computer Methods Applied Mechanics and Engineering*, vol. 191, no. 43, pp. 4927–4948, 2002.

[13] G. Wübbeler, M. Krystek, and C. Elster, "Evaluation of measurement uncertainty and its numerical calculation by a Monte Carlo method," *Measurement Science and Technology*, vol. 19, no. 8, Article ID 084009, 2008.

[14] X. Jiang and S. Mahadevan, "Bayesian hierarchical uncertainty quantification by structural equation modeling," *International Journal for Numerical Methods in Engineering*, vol. 80, no. 6-7, pp. 717–737, 2009.

[15] M. A. Navacerrada, A. Pedrero, and C. Díaz, "Study of the uncertainty of façade sound insulation measurements: Analysis of the ISO 12999-1 uncertainty proposal," *Applied Acoustics*, vol. 114, pp. 1–9, 2016.

[16] M. Hölle, C. Bartsch, and P. Jeschke, "Evaluation of measurement uncertainties for pneumatic multihole probes using a Monte Carlo method," *Journal of Engineering for Gas Turbines and Power*, vol. 139, no. 7, Article ID 072605, 2017.

[17] X. L. Wen, Y. B. Zhao, D. X. Wang, and J. Pan, "Adaptive Monte Carlo and GUM methods for the evaluation of measurement uncertainty of cylindricity error," *Precision Engineering*, vol. 37, no. 4, pp. 856–864, 2013.

[18] *Joint Committee for Guides in Metrology, Evaluation of Measurement Data-An Introduction to the "Guide to The Expression of Uncertainty in Measurement" and Related Documents*, JCGM, 2009.

[19] American Association for Laboratory Accreditation(A2LA), *G104—Guide for Estimation of Measurement Uncertainty in Testing*, 2014.

[20] *JCGM 101, Evaluation of Measurement Data — Supplement 1 to the "Guide to the Expression of Uncertainty in Measurement" —Propagation of Distributions Using A Monte Carlo Method*, JCGM member organizations (BIPM, IEC, IFCC, ILAC, ISO, IUPAC, IUPAP and OIML), 2008.

[21] *ISO 15530: Geometrical Product Specifications (GPS)—Coordinate Measuring Machines (CMM): Technique for Determining The Uncertainty of Measurement—Part 4:Evaluating Task-Specific Measurement Uncertainty Using Simulation*, 2008.

[22] J. Santolaria and M. Ginés, "Uncertainty estimation in robot kinematic calibration," *Robotics and Computer-Integrated Manufacturing*, vol. 29, no. 2, pp. 370–384, 2013.

[23] R. Li and X. Qu, "Study on calibration uncertainty of industrial robot kinematic parameters," *Chinese Journal of Scientific Instrument*, vol. 35, no. 10, pp. 2192–2199, 2014 (Chinese).

[24] A. Olarra, D. Axinte, and G. Kortaberria, "Geometrical calibration and uncertainty estimation methodology for a novel self-propelled miniature robotic machine tool," *Robotics and Computer-Integrated Manufacturing*, vol. 49, pp. 204–214, 2018.

[25] Z. S. Roth, B. W. Mooring, and B. Ravani, "An overview of robot calibration," *IEEE Transactions on Robotics and Automation*, vol. 3, no. 5, pp. 377–385, 1987.

[26] S. Hayati, "Robot arm geometric link parameter estimation," in *Proceedings of the The 22nd IEEE Conference on Decision and Control*, pp. 1477–1483, San Antonio, USA, December 1983.

[27] G. Gang, L. Tong, C. Ming, J. Q. Xuan, and S. H. Xu, "Review on kinematics calibration technology of serial robots," *International Journal of Precision Engineering and Manufacturing*, vol. 15, no. 8, pp. 1759–1774, 2014.

[28] W. Yang, J. X. Chen, and J. S. Li, "Two-step spatial circle fitting method based on projection," *Journal of Engineering Design*, vol. 16, no. 2, pp. 117–121, 2009 (Chinese).

[29] International Standard Organization, *ISO/TS 14253-2-1999 Geometrical Product Specifications (GPS)- Inspection by Measurement of Workpieces And Measuring Equipment —Part 2: Guide to the Estimation of Uncertainty in GPS Measurement, in Calibration of Measuring Equipment And in Product Verification*, ISO Copyright Office, Switzerland, 1999.

[30] K. Rost, K. Wendt, and F. Härtig, "Evaluating a task-specific measurement uncertainty for gear measuring instruments via Monte Carlo simulation," *Precision Engineering*, vol. 44, pp. 220–230, 2016.

[31] A. Giordani and L. Mari, "Measurement, models, and uncertainty," *IEEE Transactions on Instrumentation and Measurement*, vol. 61, no. 8, pp. 2144–2152, 2012.